pH-Responsive Dithiomaleimide-Amphiphilic Block Copolymer for Drug Delivery and Cellular Imaging

Ting Bai[a], Dongyan Shao[b], Jianxin Chen[a], Yifan Li[c], Ben Bin Xu[c]* and Jie Kong[a]*

[a]Shaanxi Key Laboratory of Macromolecular Science and Technology, School of Science, Northwestern Polytechnical University, Xi'an, 710072, P. R. China

[b]Key Laboratory for Space Bioscience and Biotechnology, School of Life Sciences, Northwestern Polytechnical University, Xi'an, 710072, P. R. China

[c]Mechanical and Construction Engineering, Faculty of Engineering and Environment, Northumbria University, Newcastle Upon Tyne, NE1 8ST, UK

*Corresponding Author, E-mail: kongjie@nwpu.edu.cn (J.K.) and ben.xu@northumbria.ac.uk (B.X.)

Abstract:

Drug delivery system integrated with fluorescent imaging is an emerging platform for tumor diagnostic and therapy. A pH-responsive and fluorescent polymer that could respond to the surrounding medium is a desired component to construct advanced drug delivery system with bioimaging characteristics and controllable drug release. In this work, we synthesised a novel amphiphilic block copolymers of poly(ethylene glycol)-*b*-poly(2-(diisopropylamino) ethyl methacrylate-*co*-dithiomaleimide) (PEG-*b*-poly(DPA-*co*-DTM)) and poly(ethylene glycol)-*b*-poly(2-(dibutylamino) ethyl methacrylate-*co*-dithiomaleimide) (PEG-*b*-poly(DBA-*co*-DTM)) with pH-responsiveness and fluorescence properties. The block copolymers exhibited relatively stable fluorescence property in different solvents and an excitation-independent fluorescence behavior. By copolymerizing the responsive segment in the molecule chain, the doxorubicin (DOX)-loaded micelles could be triggered to disassemble, thus releasing DOX at the corresponding pH value, yielding a pH-responsive drug release system. Targeted deliveries of drug within the cell were demonstrated by using the carrier responding to different pH values. The best antitumor effect was obtained by PEG-*b*-poly(DPA-*co*-DTM) which immediately released DOX when it entered the tumor cell, as a result of the response to the regional pH level (pH=6.3). The pH-responsive copolymers showed excellent biocompatibility with nearly 85% of cells with these fluorescent micelles surviving when the tested concentration was up to 200 μg mL^{-1}. All in all, these pH-responsive and dithiomaleimide-based fluorescent block copolymers have great potential in future cancer diagnostic and therapeutic techniques.

Keywords: dithiomaleimide, fluorescence imaging, pH-responsive, amphiphilic block copolymer, drug delivery

1. Introduction

Fluorescence imaging, a reliable strategy to detect and visualize bio-subjects both *in vitro* and *in vivo* [1-3], has led to wide applications in clinical practices [4-7]. The key features for fluorescence imaging technique, normally driven by high specification fluorescent probe, are the high sensitivity and non-radioactivity [1, 8] that can acquire feedbacks at molecular level as well as good biocompatibility [1]. Recent developments on quality fluorescence imaging suggested few technical bottlenecks, i.e., aggregation-caused quenching of traditional organic fluorophores [9-11], cytotoxicity of semiconductor Quantum Dots [12-13], low luminescence intensity of lanthanide luminescent materials [3]. Therefore, there is a timing demand to enhance and/or seek novel fluorescent probes to address the above technical gaps. At the same time, most probes mentioned above present poor water solubility and short circulation time, thus many polymer-based micelle systems have been developed for transportation of bioimaging probes [14]. For example, Zhu's group reported a glucose-based NIR-fluorescence polymer, PMMA-*b*-P(GATH-*co*-BOD) for cancer detection with strong recognition towards GLUT1 [15].

Combining bioimaging with smart drug release to get multifunctional nanomaterials is of great significance in diagnostic and therapeutic applications [16-17]. These imaging-guided drug delivery systems can visualize the accumulation of nanoparticles and simultaneously deliver and trace the drug, thereby evaluating the efficiency of drug delivery [17-18]. For molecular therapies, these nanomaterials may be able to understand the pharmacokinetic processes, which are important for nanomedicine [18]. Fluorescent and pH-responsive polymers are popular in imaging-guided drug delivery systems, being able to recognize the small pH changes around tumor microenvironment, where the pH value in early endosomes is about 5.9-6.2, but around 5.0-5.5 in the late endosomes/lysosomes [19-23]. However, advanced drug delivery strategy with high pH sensitivity and fast responsive remain yet to be fully exploited.

From the perspective of scoping novel materials, the poly(2-(diisopropylamino) ethyl methacrylate) (PDPA) and poly(2-(dibutylamino) ethyl methacrylate) (PDBA) are found to be highly sensitive to pH in early endosomes and late endosomes/lysosomes, which explain their potentials in controlled drug delivery applications [24-29]. Dithiomaleimides (DTMs) are a class of highly emissive fluorophores that possess smart ON-OFF emissive switch effect [30-31], and can be co-polymerised into fluorescent polymer-DTM [33-35] with applications in proteins-labelling [30, 36], gene delivery [30] and controlled drug release [37].

In this work, we propose a novel fluorescent and pH-responsive material strategy by co-polymerizing fluorescent DTM groups with pH-sensitive polymers (PDPA and PDBA), aiming to improve efficiency for cellular imaging and drug release. DOX-loaded micelles self-assembled from PEG-*b*-poly(DPA-*co*-DTM) or PEG-*b*-poly(DBA-*co*-DTM) were taken up by tumor cells, the pH-responsive parts became positively charged at low pH leading to dissociation of micelles into unimers and therefore releasing DOX. Simultaneously, the DTM probes exhibited bright green fluorescence to achieve cellular imaging. The drug releasing roadmap is shown in **Scheme 1**.

2. Experimental

2.1 Materials

2,3-Dibromomaleimide (98%) was purchased from Ark. Butanethiol (97%) was purchased from TCI. Propargyl bromide (98%, contains 0.3% MgO as a stabilizer), 2-bromo-2-methylpropionyl bromide (98%), 3-chloro-1-propanol (98%) and *N*, *N*, *N'*, *N'*, *N''*-pentamethyl-diethylenetriamine (PMDETA, 99%) and trimethylamine (TEA, 99.7%)were purchased from Aladdin. 2-Diisopropylaminoethanol (98%) was purchased from Adamas. Poly(ethylene glycol) methyl ether (PEG_{113}-OH, M_n = 5000)

and 2-(dibutylamino)ethanol (99%) were purchased from Aldrich and used as received. A549 cell lines were purchased from China Center for Type Culture Collection (Wuhan, China). Dulbecco's modified Eagle medium (DMEM) was purchased from HyClone. Fetal bovine medium (FBS), phosphate buffer saline (PBS) and Cell Counting Kit-8 were purchased from Beyotime. All the other reagents were available commercially from J&K Chemical and used as received. Alkyne-DTM [38-39], 3-azido propanol (AzPOH) [40-41], 3-azidopropyl methacrylate (AzPMA) [40-41], 2-(Diisopropylamino)ethyl methacrylate (DPA-MA) and 2-(Dibutylamino)ethyl methacrylate (DBA-MA) [25], as well as PEG-Br [42] were synthesized according to a previously reported method.

2.2 Synthesis of methacrylate-functional DTM (DTM-MA)

DTM-MA was synthesized via the "click" reaction. Alkyne-DTM (934.14 mg, 3 mmol), AzPMA (558.13 mg, 3.3 mmol) and PMDETA (138.4 mg, 0.8 mmol) were dissolved in 5 mL anhydrous dimethylformamide (DMF). The mixture was degassed via three freeze-evacuate-thaw cycles followed by the addition of CuBr (114.8 mg, 0.8 mmol). The solution was allowed to stir for 24 h under N_2 atmosphere at 50 °C. Then the solution was exposed to air, and diluted with dichlormethane (DCM). The mixture was then passed through a neutral alumina and the residue was purified by silica gel column chromatography (hexane : ethyl acetate = 2:1, v/v) to yield yellow liquid (1.2 g, 83%). ^{1}H NMR (400 MHz, $CDCl_3$) δ: 0.93 (-S-$(CH_2)_3$-C$\boldsymbol{H}_3$), 1.44 (-S-$(CH_2)_2$-C$\boldsymbol{H}_2$-CH_3), 1.63 (-S-CH_2-C$\boldsymbol{H}_2$-CH_2-CH_3), 1.95 (CH_2=C(C$\boldsymbol{H}_3$)-), 2.31 (-O-CH_2-C$\boldsymbol{H}_2$-CH_2-), 3.3 (-S-C$\boldsymbol{H}_2$-$(CH_2)_2$-CH_3), 4.2 (-O-C$\boldsymbol{H}_2$-), 4.45 (-O-$(CH_2)_2$-C$\boldsymbol{H}_2$-), 4.81 (-CH=CH(C$\boldsymbol{H}_2$)-), 5.62, 6.11 (C$\boldsymbol{H}_2$=C(CH_3)-), 7.58 (triozle).

2.3 Synthesis of PEG-*b*-poly(DPA-*co*-DTM) and PEG-*b*-poly(DBA-*co*-DTM) block copolymers

PEG-*b*-poly(DPA-*co*-DTM) and PEG-*b*-poly(DBA-*co*-DTM) block copolymers with different compositions were synthesized by atom transfer radical polymerization

(ATRP). Synthesis of PEG-*b*-poly(DPA-*co*-DTM) was described as a representative procedure. PEG-Br (100 mg, 0.02 mmol), DPA-MA (170.65 mg, 0.8 mmol), DTM-MA (48.05 mg, 0.1 mmol) and PMDETA (3.46 mg, 0.02 mmol) were dissolved in 2 mL anhydrous DMF. The mixture was degassed via three freeze-evacuate-thaw cycles followed by the addition of CuBr (2.87 mg, 0.02 mmol). After 12 h of stirring under an N_2 atmosphere at 60 °C, the reaction bottle was quickly quenched into an ice bath and exposed to air, then diluted with DCM. The mixture was then passed through a neutral alumina. The filtrate was concentrated and precipitated into excess cold diethyl ether twice and dried in a vacuum to yield yellowish-brown solid.

2.4 Characterization

^{1}H NMR spectra were recorded on a Bruker AV 400 NMR spectrometer with $CDCl_3$ as the solvent. Fourier transform infrared spectra (FT-IR) were recorded using a NICOLET iS10 IR spectrometer using the potassium bromide (KBr) method. The number- and weight-average molecular weight (M_n and M_w, respectively) and polydispersity index (PDI = M_w / M_n) were measured using a GPC-MALLS system equipped with a Waters 515 pump, an autosampler and two gel columns (10^3 Å and 10^4 Å, MZ, Shimadzu Co.) with a flow rate of 0.5 mL min^{-1} in THF (HPLC grade) at 25 °C. The detectors used included a differential refractometer (Optilab rEX, Wyatt) and a multiangle light scattering detector (MALLS) equipped with a 632.8 nm He-Ne laser (DAWN EOS, Wyatt). The refractive index increments (d*n*/d*c*) of polymers in THF were measured at 25 °C using an Optilab rEX differential refractometer. ASTRA software (Version 5.1.3.0) was utilized for acquisition and analysis of data. At the adjustment stage of this instrument, the polystyrene standard was used. Dynamic light scattering (DLS) measurements were made with a Zetasizer Nano-ZS (Malvern Instruments, UK). Cryo-transmission electron microscopy (cryo-TEM) was performed with a FEI Talos F200C microscope (Thermo Scientific, US) with an electron kinetic energy of 200 kV. The samples were prepared by dropping micelle solutions onto copper grids and allowed to immediately freeze in liquid N_2 overnight before

measurement. Fluorescence spectra of compounds were measured on a Hitachi F-4500 spectrophotometer equipped with a 150 W xenon lamp as the excitation source, the slit widths were both set at 5 nm for excitation and emission. The cell uptake experiment was conducted by confocal microscope (Leica TCS-SP5). Cell viability was detected by M200 Pro nanoquant (Tecan). Cell apoptosis was evaluated by Muse Cell Analyzer (Merck & Millipore, Germany).

2.5 Preparation of micelle nanoparticles

Micelles were prepared by a dialysis method. PEG-*b*-poly(DPA-*co*-DTM) (40 mg) was dissolved in 1.5 mL DMF for 20 min, then 4 mL deionized water was added slowly to the above solution. After another stirring for 2 h, the mixture was dialyzed against deionized water for 36 h (3500 Da), and the water was replaced every 4 h. The obtained solution was filtered through 0.45 μm microfilter and lyophilized. And for drug-loaded micelles, the preparation procedure was under dark environment all the time. PEG-*b*-poly(DPA-*co*-DTM) (40 mg) and DOX (15 mg) were dissolved together in 2 mL DMF by stirring for 30 min, then 5 mL deionized water was added slowly to the above solution. After further stirring for 2 h, the mixture was filtered to remove precipitated DOX and dialyzed against deionized water for 36 h (3500 Da), and the water was replaced every 4 h. The obtained solution was then lyophilized. And for PEG-*b*-poly(DBA-*co*-DTM) micelle and DOX-loaded PEG-*b*-poly(DBA-*co*-DTM) micelle, the preparation methods were as the same. Then PEG-*b*-poly(DPA-*co*-DTM) micelle, PEG-*b*-poly(DBA-*co*-DTM) micelle, DOX-loaded PEG-*b*-poly(DPA-*co*-DTM) micelle as well as DOX-loaded PEG-*b*-poly(DBA-*co*-DTM) micelle were named as **P1** micelles, **P2** micelles, DOX-loaded **P1** micelles, and DOX-loaded **P2** micelles in the following parts.

2.6 *In vitro* drug release from DOX-loaded micelles

Freeze-dried DOX-loaded **P1** micelles and DOX-loaded **P2** micelles were dispersed in 0.1 M citric acid-sodium phosphate buffer solution (pH 7.4 and pH 6.0 for DOX-

loaded **P1** micelles; pH 7.4 and pH 5.0 for DOX-loaded **P2** micelles) respectively and transferred into dialysis membrane (3500 Da) immersed in 50mL of citric acid-sodium phosphate buffer solution at 37 °C. At predetermined intervals, 3 mL of the external medium was collected and replaced with the same volume of fresh buffer solution. UV-vis absorption at the wavelength of 488 nm was employed to assay DOX content to determine the drug loading efficiency (DLE), drug loading content (DLC), and the DOX release rate. And the release experiments were conducted in triplicate. The DLE (%) and DLC (%) was calculated as

DLE (wt%)= (weight of loaded drug/weight of drug in feed) ×100%

DLC (wt%)= (weight of loaded drug/weight of polymer and drug) ×100%

2.7 Cellular uptake

A549 cells in DMEM supplemented with 10% FBS were seeded into two 6-well plates at a density of 1 x 10^4 cells per well and cultured for 24h at 37 °C in CO_2/air (5/95, v/v). The prepared **P1** micelles, **P2** micelles, DOX-loaded **P1** micelles and DOX-loaded **P2** micelles were added at a final DTM group concentration of 10 μg mL^{-1} respectively. After further incubation for 15 min, 45 min, or 3 h, these cells were washed with PBS for three times. Then the cells were fixed for 10 min. Finally, the cells were washed with PBS again and observed with confocal microscope.

2.8 *In vitro* cytotoxicity assay

The *in vitro* cytotoxicity of **P1** micelles and the viability of A549 cells treated with free DOX and DOX-loaded **P1** micelles were evaluated by the Cell Counting Kit (CCK-8) assay. A549 cells in DMEM supplemented with 10% FBS were seeded into 96-well plates at a density of 1 x 10^4 cells per well and cultured for 24h at 37 °C in CO_2/air (5/95, v/v). Then, the cells were cultured with medium containing various concentrations of **P1** micelles from 25 to 200 μg mL^{-1} as well as free DOX and DOX-loaded **P1** micelles with final DOX concentration ranging from 1 to 20 μg mL^{-1}. After the cells were incubated for 24 h or 48 h, 10 μL of CCK-8 solution were added to each

well and the cells were incubated for another 2h at 37 °C. The cell viability was determined by a microplate reader of absorbance at 450 nm. The *in vitro* cytotoxicity of **P2** micelles and the viability of A549 cells treated with free DOX and DOX-loaded **P2** micelles were evaluated as the same methods.

2.9 *In vitro* apoptosis

For cell apoptosis assay, A549 cells were cultured in a six-well plate and further grown for 24 h. Then, the cells were treated with pure **P1** micelles, **P2** micelles, DOX-loaded **P1** and DOX-loaded **P2** micelles, respectively. After 24 h of incubation, all attached and floating cells were collected, and mixed with 50 μL of Muse^{TM} annexin V & Dead Cell Reagent for 10 min in the darkness at room temperature. Then, the samples were detected by Muse Cell Analyzer.

3. Results and discussion

3.1 Synthesis and characterization of block copolymers

The fluorescent and pH-responsive amphiphilic block copolymers of PEG-*b*-poly(DPA-*co*-DTM) and PEG-*b*-poly(DBA-*co*-DTM) were synthesized according to **Scheme 1**. DTM was first modified into a DTM-MA monomer, and then the macroinitiator PEG-Br initiated the atom transfer radical polymerization (ATRP) of DTM-MA and DPA-MA or DBA-MA to get block copolymers with PEG as the hydrophilic part and the fluorescent DTMs incorporated into the pH-responsive parts. The length of the PDPA segments and PDBA segments in block copolymers was tuned by controlling the polymerization process. PEG_{113}-*b*-poly(DPA_{80}-*co*-DTM_5) and PEG_{113}-*b*-poly(DBA_{80}-*co*-DTM_5) copolymers are named **P1** and **P2** respectively.

The stepwise synthesis of DTM-MA monomer could be verified by ^{1}H NMR and FT-IR results. The ^{1}H NMR confirmed the synthesis of AzPMA by the disappearance of a signal at 2.0 ppm (hydroxyl group) and the onsite of double bond peaks at 5.6 ppm

and 6.1 ppm (**Figure S1-S2**). The triazole group signal at 7.6 ppm appeared in the ^{1}H NMR proved the successful synthesis of DTM-MA (**Figure 1A** and **S3**). The infrared spectra (**Figure 1C**) evidenced the synthesis of AzPMA from the disappearance of hydroxyl group peak at 3334 nm^{-1} and the onsite of ketone group at 1720 nm^{-1}, and the formation of DTM-MA from the disappearances of the alkynyl group peak at 3189 nm^{-1} and N_3 group at 2100 nm^{-1}.

The chemical structure for synthesized block copolymers were also characterized. For **P1** (**Figure 1B**), the peaks at 3.0 ppm and 2.6 ppm associated with the methylene and methine next to the nitrogen atom in the PDPA and the peak at 7.6 ppm referred to the triazole group in the PDTM proved the block copolymers formation. Whereas for **P2** (**Figure S4**), the peaks referred to the methylene next to the nitrogen atom in the PDBA were found at 2.5-2.7 ppm, and at 7.6 ppm for the triazole group in the PDTM. The molecular weight results measured by GPC and NMR are shown in **Table S1** and **Figure 1D**. The M_n of the polymers **P1**and **P2** were 24.3 kDa and 26.1 kDa, the PDI were 1.28 and 1.21 respectively, which agreed well with the theoretical molecular weights calculated by ^{1}H NMR.

Particle size is an important property of polymeric micelles for drug delivery and release. For the designed amphiphilic block copolymers **P1** and **P2**, the hydrophilic segment PEG is the shell and the hydrophobic segment P(DPA-*co*-DTM) or P(DBA-*co*-DTM) is the core of the micelle. DLS results of intensity indicated that the size distributions were 28±8 nm and 37±6 nm for **P1** and **P2** micelles, whereas the cryo-TEM results showed smaller size distributions at 16±2 nm and 27±4 nm (**Figure 2a** and **2b**). After loading DOX into the micelles, cryo-TEM observations for DOX-loaded **P1** micelles and DOX-loaded **P2** micelles revealed that the size distributions were 27±5 nm and 36±8 nm, which were also smaller than the DLS results (39±10 nm for DOX-loaded **P1** micelles and 47±15 nm for DOX-loaded **P2** micelles) (**Figure 2c** and **2d**). After encapsulating the drug into the micelles, the size distributions of DLS showed approximately a 30% increment for DOX-loaded **P1** micelles and 21% increment for DOX-loaded **P2** micelles. However, both

DOX-loaded micelles were within 200 nm, therefore could penetrate and accumulate in tumor tissues through the enhanced permeability and retention (EPR) effect [43-44].

As it is well known, the PDPA and PDBA polymers hold pH-responsive properties, with a sharp pH responsive transition from hydrophobic to hydrophilic responding to pH changes from 7.4 to 6.3 (for PDPA) and from 7.4 to 5.4 (for PDBA), respectively [25]. To assess the micelle stability at different pH levels of **P1** and **P2** micelles, we measured the size changes of the micelles (**Figure 3a, 3c and Figure S6**) in citric acid-sodium phosphate buffer solution with polymer concentration of 1 mg mL^{-1} at different pH values. Under a pH of 7.4, the observed hydrodynamic diameters of both micelles were about 30-40 nm and remained constant over 36 h. However, the size of both micelles showed obvious changes after 0.5 h at the pH value of 6.0 and 5.0, which could be attributed to the charge transition of the hydrophobic segments with tertiary amines at low pH, yielding the micelle dissociation [25, 45]. This characteristic was also confirmed by cryo-TEM, when the pH was altered to 6.0 or 5.0, there were almost no spherical nanoparticles with normal size after 30 min of incubation (**Figure 3b and 3d**).

2.2 *In vitro* drug release

Recent studies reveals that pH value in tumor issues is a little lower than in normal tissues, which is beneficial for targeting applications. The intracellular pH value is lower than extracellular, typically 5.9-6.2 at early endosomes and 5.0-5.5 at late endosomes/lysosomes [19-21]. During the *in vitro* drug release characterization, the analytical results from DLC and DLE equations indicated that the drug loading content and encapsulation efficiency of the DOX-loaded **P1** micelles and DOX-loaded **P2** micelles were determined to be 22.5%, 92.1% and 16.1%, 76.3%, respectively. Thus, the *in vitro* drug release experiments were evaluated at corresponding responsive pH range, i.e. pH 7.4 and 6.0 for DOX-loaded **P1** micelles and pH 7.4 and 5.0 for DOX-loaded **P2** micelles.

At a pH value of 7.4 (**Figure 4**), the DOX releasing efficiencies remained relative stable with less than 30% from both the DOX-loaded **P1** and **P2** micelles in 36 h. At pH 6.0, we observed an acceleration of drug releasing for DOX-loaded **P1** micelles, where approximate 53% of the loaded DOX were released in the first 12 h, then it climbed up to 72% at 36 h. Similarly, approximate 42% of DOX were released from DOX-loaded **P2** micelles in the first 12 h, then the releasing rate reached 69% at 36 h. These evidenced that the micelles produced in this work presented accelerated drug release behavior at corresponding lower pH values.

2.3 Fluorescence spectroscopy

When two alkyl thiol groups are added into a non-fluorescence dibromomaleimide molecule, the correspondent dithiomaleimide molecule will be formed with strong fluorescence signal [30]. The mechanism was previously reported by other researchers that thiol groups could saturate the C=C double bond of the maleimide, subsequently eliminating the quenching of the fluorophore and eventually making the fluorophore excitative [46]. The above mechanism also applies in our **P1** and **P2** copolymers.

We assessed the fluorescence property of our samples. Under methanol environment (**Figure 5a**), the maximum excitation wavelength of both **P1** and **P2** copolymers were observed at 405 nm, and the maximum emission wavelength were at 550 nm, which was in a good agreement with that of DTM-MA monomer. In DI-water (**Figure 5b**), the maximum excitation wavelength showed no shift, however, there was a little shift from 550 nm to 520 nm for maximum emission wavelength, known as a solvatochromic emission with a blue-shift when changing solvent polarity [46]. The solvents affected not only the emission wavelength, but also the intensity of emission wavelength. When copolymer **P1** and **P2** were dissolved in H_2O/DMF mixture with different water fractions (f_w), the samples exhibited proportional fluorescence quenching, and the emission intensity just decreased to a constant value instead of fully quenching (**Figure S7-S8**). These obvious fluorescence quenching might be greatly caused by the hydrogen bonding between water and the carbonyl moiety of DTM group [46-47]. And

after exposing at a UV light of 365 nm, our samples exhibited visible green fluorescence (**Figure 5c**).

2.4 Cellular uptake and cytotoxicity

The cellular uptake experiments were performed for both **P1** and **P2** micelles against A549 cells to understand the dynamic fluorescence behavior at practical cell environment [48]. For pure micelles, a weak green fluorescence signal appeared in A549 cells at incubation time of 15 min and enhanced green fluorescence intensities were discovered at 45 min and 3 h (**Figure S9**). For DOX-loaded **P1** and **P2** micelles (**Figure 6**), no fluorescence signals could be found at 15 min as no drug-loaded copolymers entered in A549 cells. Clear fluorescence signals were observed after 45 min and 3 h of incubation duration, implying successful engagement between A549 cells and the drug-loaded micelles. The intracellular distribution of copolymers and DOX indicated a clear potential to use these materials as fluorescent probes.

The biocompatibility and cytotoxicity for pure micelles, free DOX and DOX-loaded micelles were assessed in the cell viability experiments by using Cell Counting Kit 8 (CCK-8) assay. In **Figure 7a** and **7b**, the DOX-loaded **P1** and **P2** micelles presented an efficient antitumor activity against A549 cells after incubation time of 24 h and 48 h. The concentration- and time-dependent toxicity were reflected by the reduction of cell viability when the incubation time increased and the DOX concentration increased from 1 to 20 μg mL^{-1}. Results for pure **P1** and **P2** micelles suggested an excellent biocompatibility with nearly 85 % of cells with these fluorescent micelles surviving when the tested concentration was up to 200 μg mL^{-1} (**Figure 7c)**.

The antitumor efficiencies for DOX and DOX-loaded micelles were evaluated by comparing the cell viability results after a fixed incubation period of 48 h, as shown in **Figure 7d**. DOX-loaded **P1** micelles showed the lowest cell viability towards A549 cells in all DOX concentrations, because the PDPA segment in **P1** copolymer, responding at pH of 6.3, would immediately release DOX when micelles entered into

the tumor cells where were occupied by the early endosomes (pH=6.3), thus resulting into an effective longer drug toxicity to kill tumor cells. Due to the lower pH responsive transition (pH=5.4) from PDBA, DOX-loaded **P2** micelles needed to reach late endosomes/lysosomes (pH=5.4) to release the DOX. Reaching late endosomes/lysosomes took more time by intracellular diffusion constant controlled travelling than early endosomes, therefore leading to a low antitumor efficiency. Similarly, the results from free DOX also indicated a low antitumor efficiency, resulting from the diffusion-controlled transportation from extracellular matrix to intracellular system for drug [49].

To further investigate the biocompatibility of copolymers and cytotoxicity of DOX-loaded micelles, Annexin V-PE/7-AAD apoptosis detection assay was used. **Figure 7e-7h** shows a total apoptotic ratio (sum of early apoptotic ratio, late apoptotic ratio and dead ratio) of A549 cells were collected at 3.05% (**P1** micelles), 5.94% (**P2** micelles), 31.17% (DOX-loaded **P1** micelles), and 23.61% (DOX-loaded **P2** micelles) after an incubation time of 24 h. Pure micelles had little toxicity towards A549 cells as more live cells were detected, which agreed well with the results from CCK-8 assay testing. On the other hand, high rates of apoptosis were observed for DOX-loaded micelles, where an apoptosis ratio of 26.19% was found for DOX-loaded **P1** micelles and an apoptosis ratio of 19.31% for DOX-loaded **P2** micelles. The results were in a good agreement with cytotoxicity profiles where DOX-loaded **P1** micelles had a higher antitumor efficiency to A549 cells than DOX-loaded **P2** micelles.

4. Conclusions

In summary, we successfully developed two fluorescent pH-responsive block copolymers with a robust fluorescence performance that could resist the solvent intervention. The DOX-loaded **P1** micelles show the best antitumor effect by immediately releasing DOX once entering the tumor cells, as a result of the response to the regional pH level (pH=6.3). This early release of drug not only extends the working

time for the drug but also kinetically enhances the toxicity to kill cancer cells. Moreover, both of the copolymers PEG-*b*-Poly(DPA-*co*-DTM) and PEG-*b*-Poly(DBA-*co*-DTM) show excellent biocompatibility with nearly 85 % of cells with these fluorescent micelles surviving when the tested concentration is up to 200 μg mL^{-1}. Comparing to previous studies [39, 44], this work presents higher drug loading, smarter responsiveness to microenvironment and great fluorescence performance. With superior fluorescence property and sensitive pH-responsive drug release property, we expect these polymeric micelles technology can find potential applications in biomedical and clinical therapies.

Conflicts of interest

There are no conflicts to declare.

Acknowledgements

This work was financially supported by the National Natural Science Foundation of China (21604065/21374089), Shaanxi Natural Science Funds for Distinguished Young Scholars (2018JC-008), Innovation Foundation for Doctor Dissertation of Northwestern Polytechnical University (CX201837), Fundamental Research Funds for the Central Universities (3102018jgc010), China Postdoctoral Science Foundation (2018T111098/2017M613211) and the Engineering and Physical Sciences Research Council (EPSRC) grant-EP/N007921/1.

References

[1] M. Gao, F.B. Yu, C.J. Lv, J. Choo, L.X. Chen, Fluorescent chemical probes for accurate tumor diagnosis and targeting therapy, Chem. Soc. Rev. 46 (2017) 2237-2271.

[2] B.R. Smith, S.S. Gambhir, Nanomaterials for in vivo imaging, Chem. Rev. 117 (2017) 901-986.

[3] B. Pelaz, C. Alexiou, R.A. Alvarez-Puebla, F. Alves, A.M. Andrews, S. Ashraf, L.P. Balogh, L. Ballerini, A. Bestetti, Diverse applications of nanomedicine, ACS Nano 11 (2017) 2313-2318.

[4] L. Yuan, W.Y. Lin, K.B. Zheng, L.W. He, W.M. Huang, Far-red to near infrared analyte-responsive fluorescent probes based on organic fluorophore platforms for fluorescence imaging, Chem. Soc. Rev. 42 (2013) 622-661.

[5] O.S. Wolfbeis, An overview of nanoparticles commonly used in fluorescent bioimaging, Chem. Soc. Rev. 44 (2015) 4743-4768.

[6] Y.M. Yang, Q. Zhao, W. Feng, F.Y. Li, Luminescent chemodosimeters for bioimaging, Chem. Rev. 113 (2013) 192-270.

[7] M. Vendrell, D.T. Zhai, J.C. Er, Y.T. Chang, Combinatorial strategies in fluorescent probe development, Chem. Rev. 112 (2012) 4391-4420.

[8] D.L. Wang, T.Y. Zhao, X.Y. Zhu, D.Y. Yan, W.X. Wang, Bioapplications of hyperbranched polymers, Chem. Soc. Rev. 44 (2015) 4023-4071.

[9] R.Y. Zhan, Y.T. Pan, P.N. Manghnani, B. Liu, AIE polymers: synthesis, properties, and biological applications, Macromol. Biosci. 17 (2017) 1600433-1600452.

[10] R.R. Hu, N.L.C. Leung, B.Z. Tang, AIE macromolecules: syntheses, structures and functionalities, Chem. Soc. Rev. 43 (2014) 4494-4562.

[11] B. Guo, X.L. Cai, S.D. Xu, S.M.A. Fateminia, J. Liu, J. Liang, G.X. Feng, W.B. Wu, B. Liu, Decoration of porphyrin with tetraphenylethene: converting a fluorophore with aggregation-caused quenching to aggregation-induced emission enhancement, J. Mater. Chem. B 4 (2016) 4690-4695.

[12] A.M. Derfus, W.C.W. Chan, S.N. Bhatia, Probing the cytotoxicity of semiconductor quantum dots, Nano Letters 4 (2004) 11-18.

[13] R.A. Hardman, A toxicologic review of quantum dots: toxicity depends on physicochemical and environmental factors, Environ. Health. Perspect. 114 (2006) 165-172.

[14] J.H. Kim, K. Park, H.Y. Nam, S. Lee, K. Kim, I.C. Kwon, Polymers for bioimaging,

Prog. Polym. Sci. 32 (2007) 1031-1053.

[15] Y.J. Zhao, Y. Wu, B. Xue, X. Jin, X.Y. Zhu, Novel target NIR-fluorescent polymer for living tumor cell imaging, Polym. Chem. 10 (2019) 77-85.

[16] Y. Hu, S. Mignani, J.P. Majoral, M.W. Shen, X.Y. Shi, Construction of iron oxide nanoparticle-based hybrid platforms for tumor imaging and therapy, Chem. Soc. Rev. 47 (2018) 1874-1900.

[17] X.G. Liu, M. Wu, Q.L. Hu, H.Z. Bai, S.Q. Zhang, Y.Q. Shen, G.P. Tang, Y. Ping, Precise imaging-guided cancer therapy and real-time pharmacokinetic monitoring, ACS Nano, 10 (2016) 11385-11396.

[18] A. Gianella, P.A. Jarzyna, V. Mani, S. Ramachandran, C. Calcagno, J. Tang, B. Kann, W.J.R. Dijk, V.L. Thijssen, A.W. Griffioen, G. Storm, Z.A. Fayad, W.J.M. Mulder, Multifunctional nanoemulsion platform for imaging guided therapy evaluated in experimental cancer, ACS Nano, 5 (2011) 4422-4433.

[19] J.Y. Han, K. Burgess, Fluorescent indicators for intracellular pH, Chem. Rev. 110 (2010) 2709-2728.

[20] J.T. Hou, W.X. Ren, K. Li, J. Seo, A. Sharma, X.Q. Yu, J.S. Kim, Fluorescent bioimaging of pH: from design to applications, Chem. Soc. Rev. 46 (2017) 2076-2090.

[21] L.Y. Fu, P. Yuan, Z. Ruan, L. Liu, T.W. Li, L.F. Yan, Ultra-pH-sensitive polypeptide micelles with large fluorescence off/on ratio in near infrared range, Polym. Chem. 8 (2017) 1028-1038.

[22] M.L. Wei, Y.F. Gao, X. Li, M.J. Serpe, Stimuli-responsive polymers and their applications, Polym. Chem. 8 (2017) 127-143.

[23] S.L. Li, K.L. Hu, W.P. Cao, Y. Sun, W. Sheng, F. Li, Y. Wu, X.J. Liang, pH-Responsive biocompatible fluorescent polymer nanoparticles based on phenylboronic acid for intracellular imaging and drug delivery, Nanoscale 6 (2014) 13701-13709.

[24] G. Kocak, C. Tuncer, V. Bütün, pH-Responsive polymers, Polym. Chem. 8 (2017) 144-176.

[25] K.J. Zhou, Y.G. Wang, X.N. Huang, K. Luby-Phelps, B.D. Sumer, J.M. Gao, Tunable, ultrasensitive pH-responsive nanoparticles targeting specific endocytic organelles in living cells, Angew. Chem. Int. Ed. 50 (2011) 6109-6114.

[26] K.J. Zhou, H.M. Liu, S.R. Zhang, X.N. Huang, Y.G. Wang, G. Huang, B.D. Sumer, J.M. Gao, Multicolored pH-tunable and activatable fluorescence nanoplatform responsive to physiologic pH stimuli, J. Am. Chem. Soc. 134 (2012) 7803-7811.

[27] X.P. Ma, Y.G. Wang, T. Zhao, Y. Li, L.C. Su, Z.H. Wang, G. Huang, B.D. Sumer, J.M. Gao, Ultra-pH-sensitive nanoprobe library with broad pH tunability and fluorescence emissions, J. Am. Chem. Soc. 136 (2014) 11085-11092.

[28] Y.G. Wang, C.S. Wang, Y. Li, G. Huang, T. Zhao, X.P. Ma, Z.H. Wang, B.D. Sumer, M.A. White, J.M. Gao, Digitization of endocytic pH by hybrid ultra-pH-sensitive nanoprobes at single-organelle resolution, Adv. Mater. 29 (2017) 1603794-1603802.

[29] X.D. Xu, J. Wu, Y.L. Liu, M. Yu, L.L. Zhao, X. Zhu, S. Bhasin, Q. Li, E. Ha, J.J. Shi, O.C. Farokhzad, Ultra-pH-responsive and tumor-penetrating nanoplatform for targeted siRNA delivery with robust anti-cancer efficacy, Angew. Chem. Int. Ed. 55 (2016) 7091-7094.

[30] M.P. Robin, P. Wilson, A.B. Mabire, J.K. Kiviaho, J.E. Raymond, D.M. Haddleton, R.K. O'Reilly, Conjugation-induced fluorescent labeling of proteins and polymers using dithiomaleimides, J. Am. Chem. Soc. 135 (2013) 2875-2878.

[31] A.B. Mabire, M.P. Robin, H. Willcock, A. Pitto-Barry, N. Kirby, R.K. O'Reilly, Dual effect of thiol addition on fluorescent polymeric micelles: ON-to-OFF emissive switch and morphology transition, Chem. Commun. 50 (2014) 11492-11495.

[32] M.P. Robin, A.B. Mabire, J.C. Damborsky, E.S. Thom, U.H. Winzer-Serhan, J.E. Raymond, R.K. O'Reilly, New functional handle for use as a self-reporting contrast and delivery agent in nanomedicine, J. Am. Chem. Soc. 135 (2013) 9518-9524.

[33] M.P. Robin, R.K. O'Reilly, Fluorescent and chemico-fluorescent responsive polymers from dithiomaleimide and dibromomaleimide functional monomers, Chem. Sci. 5 (2014) 2717-2723.

[34] M.P. Robin, J.E. Raymond, R.K. O'Reilly, One-pot synthesis of super-bright fluorescent nanogel contrast agents containing a dithiomaleimide fluorophore, Mater. Horiz. 2 (2015) 54-59.

[35] M.P. Robin, S.A.M. Osborne, Z. Pikramenou, J.E. Raymond, R.K. O'Reilly, Fluorescent block copolymer micelles that can self-report on their assembly and small molecule encapsulation, Macromolecules 49 (2016) 653-662.

[36] M.W. Jones, R.A. Strickland, F.F. Schumacher, S. Caddick, J.R. Baker, M.I. Gibson, D.M. Haddleton, Highly efficient disulfide bridging polymers for bioconjugates from radical-compatible dithiophenol maleimides, Chem. Commun. 48 (2012) 4064-4066.

[37] L. Castañeda, A. Maruani, F.F. Schumacher, E. Miranda, V. Chudasama, K.A. Chester, J.R. Baker, M.E.B. Smith, S. Caddick, Acid-cleavable thiomaleamic acid linker for homogeneous antibody-drug conjugation, Chem. Commun. 49 (2013) 8187-8189.

[38] H. Wang, M. Xu, M.H. Xiong, J.J. Cheng, Reduction-responsive dithiomaleimide-based nanomedicine with high drug loading and FRET-indicated drug release, Chem. Commun. 51 (2015) 4807-4810.

[39] T. Bai, J.J. Du, J.X. Chen, X. Duan, Q. Zhuang, H. Chen, J. Kong, Reduction-responsive dithiomaleimide-based polymeric micelles for controlled anti-cancer drug delivery and bioimaging, Polym. Chem. 8 (2017) 7160-7168.

[40] O. Bertrand, B. Ernould, F. Boujioui, A. Vladb, J.F. Gohy, Synthesis of polymer precursors of electroactive materials by SET-LRP, Polym. Chem. 6 (2015) 6067-6072.

[41] Z.F. Jia, V.A. Bobrin, N.P. Truong, M. Gillard, M.J. Monteiro, Multifunctional nanoworms and nanorods through a one-step aqueous dispersion polymerization, J. Am. Chem. Soc. 136 (2014) 5824-5827.

[42] X.D. Xu, J. Wu, Y.L. Liu, M. Yu, L.L. Zhao, X. Zhu, S. Bhasin, Q. Li, E. Ha, J.J. Shi, O.C. Farokhzad, Ultra-pH-responsive and tumor-penetrating nanoplatform for targeted siRNA delivery with robust anti-cancer efficacy, Angew. Chem. Int. Ed. 55 (2016) 7091-7094.

[43] Q.F. Ban, T. Bai, X. Duan, J. Kong, Noninvasive photothermal cancer therapy nanoplatforms via integrating nanomaterials and functional polymers, Biomater. Sci. 5 (2017) 190-210.

[44] X. Duan, T. Bai, J.J. Du, J. Kong, One-pot synthesis of glutathione-responsive amphiphilic drug self-delivery micelles of doxorubicin-disulfide-methoxy polyethylene glycol for tumor therapy, J. Mater. Chem. B 6 (2018) 39-43.

[45] M.M. Huang, K.J. Zhao, L. Wang, S.Q. Lin, J.J. Li, J.B. Chen, C.G. Zhao, Z.S. Ge, Dual stimuli-responsive polymer prodrugs quantitatively loaded by nanoparticles for enhanced cellular internalization and triggered drug release, ACS Appl. Mater. Interfaces 8 (2016) 11226-11236.

[46] A.B. Mabire, M.P. Robin, W.D. Quan, H. Willcock, V.G. Stavros, R.K. O'Reilly, Aminomaleimide fluorophores: a simple functional group with bright, solvent dependent emission, Chem. Commun. 51 (2015) 9733-9736.

[47] Q.H. Zhu, Z.W. Ye, W.J. Yang, X.T. Cai, B.Z. Tang, One-pot synthesis and structure-property relationship of aminomaleimides: fluorescence efficiencies in monomers and aggregates easily tuned by switch of aryl and alkyl, J. Org. Chem. 82 (2017) 1096-1104.

[48] L.L. Wu, X.L. Li, Y.F. Ling, C.S. Huang, N.Q. Jia, Morpholine derivative-functionalized carbon dots-based fluorescent probe for highly selective lysosomal imaging in living cells, ACS Appl. Mater. Interfaces 9 (2017) 28222-28232.

[49] D.W. Li, Y.Z. Bu, L.N. Zhang, X. Wang, Y.Y. Yang, Y.P. Zhuang, F. Yang, H. Shen, D.C. Wu, Facile construction of pH- and redox-responsive micelles from a biodegradable poly(β-hydroxyl amine) for drug delivery, Biomacromolecules 17 (2016) 291-300.

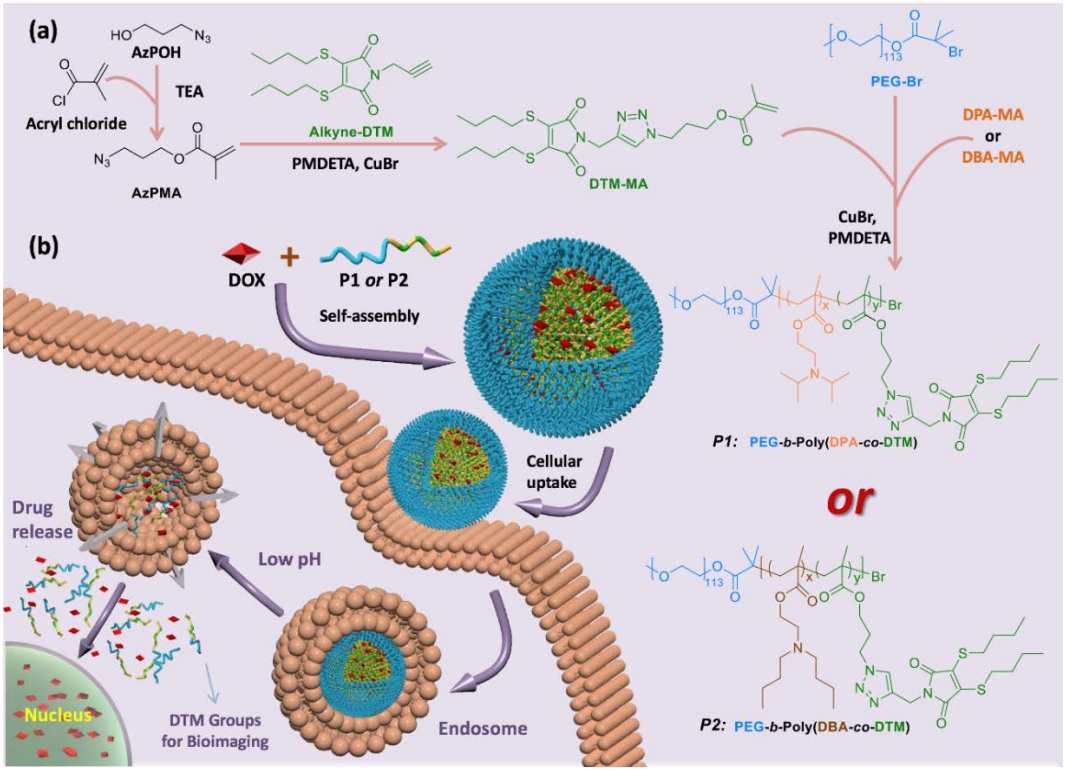

Scheme 1. Schematic for preparation of fluorescent dithiomaleimide-amphiphilic block copolymers, PEG-*b*-poly(DPA-*co*-DTM) and PEG-*b*-poly(DBA-*co*-DTM) (a), and illustration of pH responsive drug delivery into a tumor cell (b).

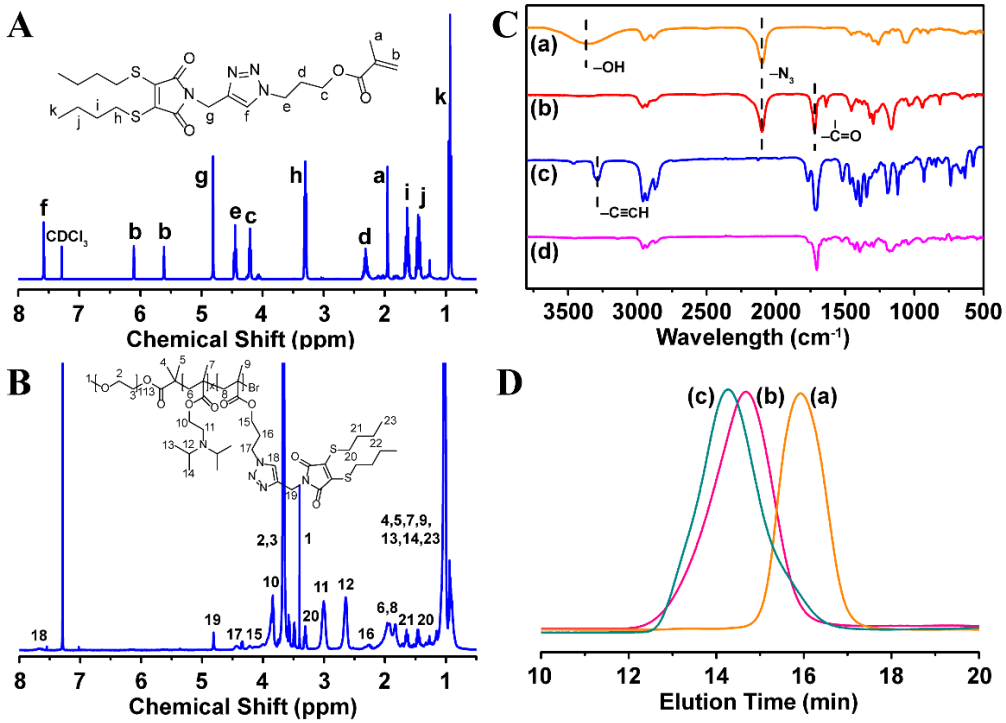

Figure 1. ^{1}H NMR spectra of DTM-MA (A) and **P1** (B) in chloroform; FT-IR spectra of (a) AzPOH, (b) AzPMA, (c) alkyne-DTM and (d) DTM-MA (C); GPC traces of (a) PEG-Br, (b) **P1**, (c) **P2** (D).

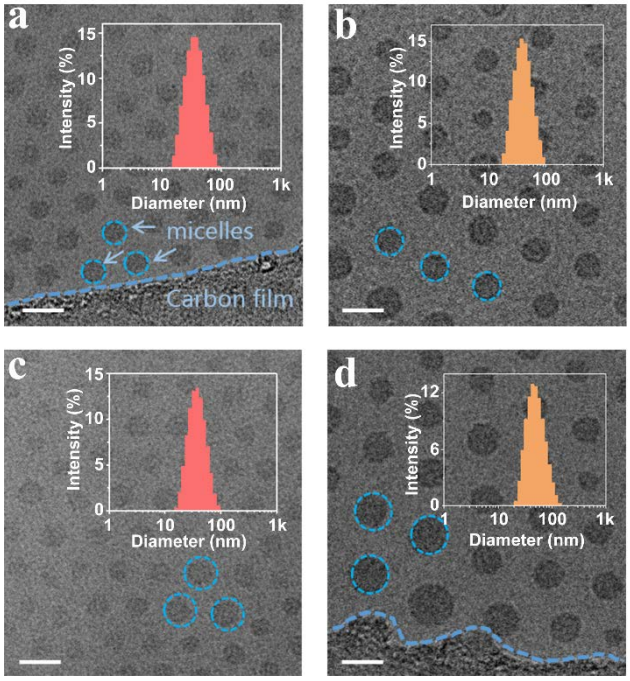

Figure 2. Cryo-TEM images of (a) **P1** micelles, (b) **P2** micelles, (c) DOX-loaded **P1** micelles, (d) DOX-loaded **P2** micelles. (scale bar=30 nm) Inset: DLS characterization.

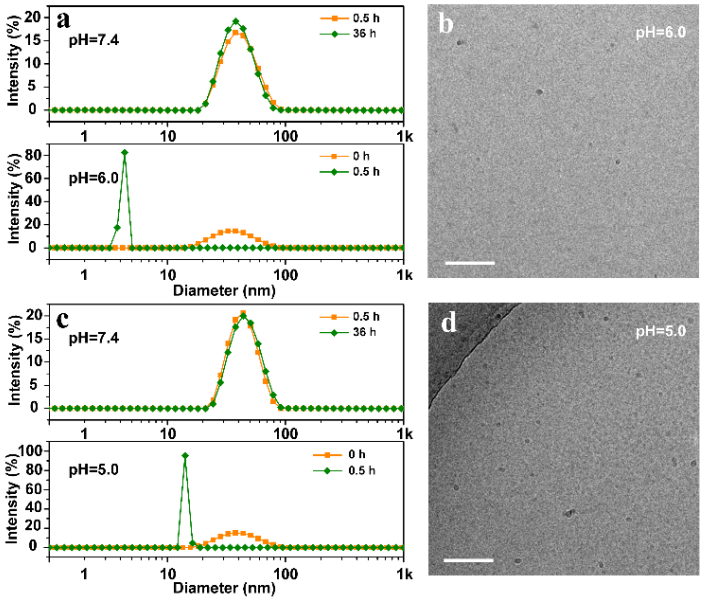

Figure 3. (a) Size change for **P1** micelles at pH=7.4 and pH=6.0, within 0.1 M citric acid-sodium phosphate buffer solution (37 °C); (b) cryo-TEM images of **P1** micelles at pH=6.0 (scale bar=50 nm); (c) size change for **P2** micelles at pH=7.4 and pH=5.0, within 0.1 M citric acid-sodium phosphate buffer solution (37 °C); (d) cryo-TEM images of **P2** micelles at pH=5.0 (scale bar=50 nm).

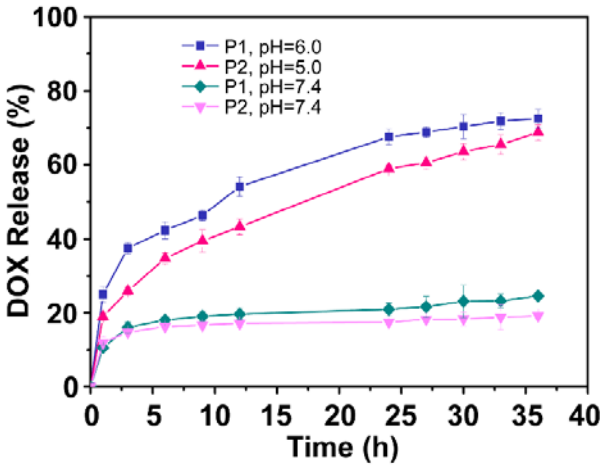

Figure 4. DOX release profiles from DOX-loaded micelles in citric acid-sodium phosphate buffer solution (0.1 M, 37 °C). Data are presented as mean ± SD (n = 3).

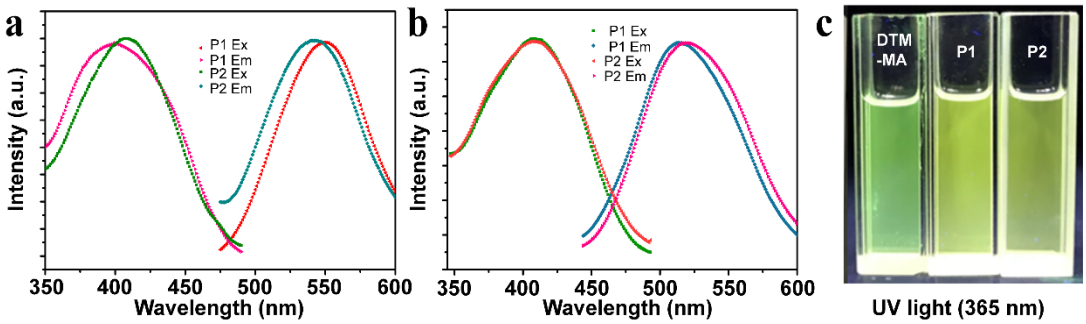

Figure 5. Fluorescence excitation and emission spectra of both **P1** and **P2** copolymers in (a) methanol, and (b) deionized water. (c) Photographs of DTM-MA (2 x 10^{-5} M), **P1** copolymer (0.3 mg ml^{-1}) and **P2** copolymer (0.3 mg ml^{-1}) dissolved in dichlormethane (DCM), taken under UV light (365 nm).

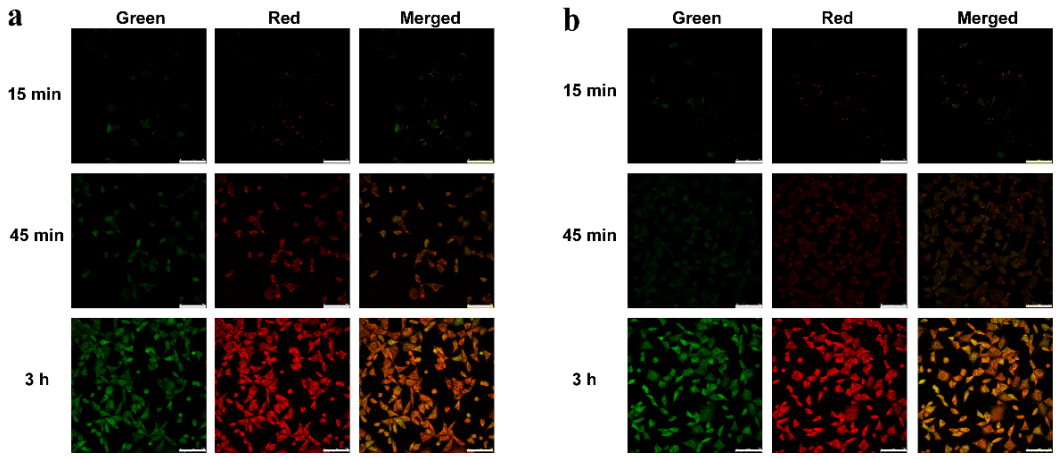

Figure 6. Fluorescence microscopy images of A549 cells after incubation of DOX loaded (a) **P1** and (b) **P2** micelles for 15 min, 45 min and 3 h. (Scale bar=75 μm)

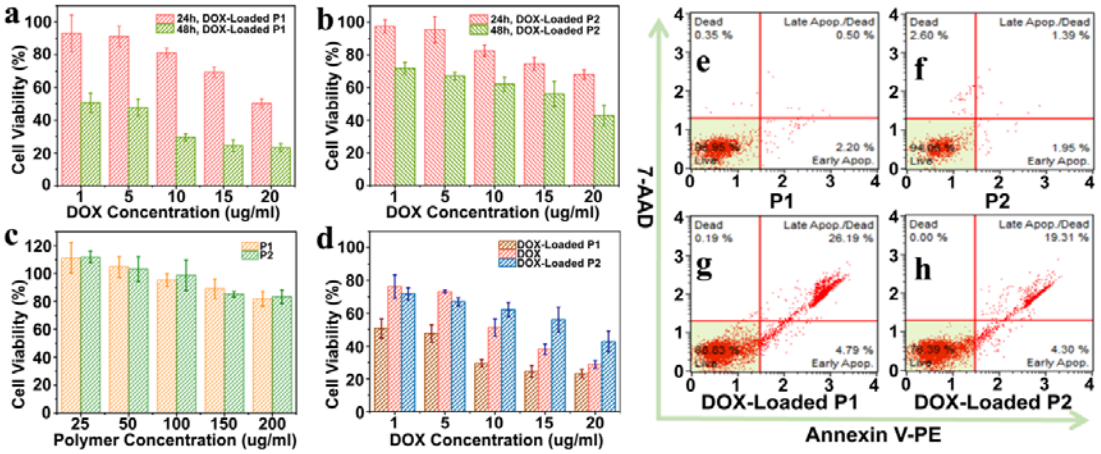

Figure 7. Cell viability results with (a) DOX-loaded **P1** micelles and (b) DOX-loaded **P2** micelles for 24 h and 48h incubations at varying DOX concentrations, (c) **P1** micelles and **P2** micelles after 24 h incubation, (d) free DOX, DOX-loaded **P1** and DOX-loaded **P2** micelles for 48 h incubation at varying equivalent DOX concentrations (n = 3). A549 Cell apoptosis analysis induced by (e) **P1** micelles, (f) **P2** micelles, (g) DOX-loaded **P1** micelles, (h) DOX-loaded **P2** micelles for 24 h incubation.

Graphical abstract